Influence of Supersaturation and Spontaneous Catalyst Formation on the Growth of PbS Wires: Toward a Unified Understanding of Growth Modes

Patricia L. Nichols,[†,‡] Minghua Sun,[‡] and Cun-Zheng Ning[‡,*]

[†]Materials Science and Engineering, School for Engineering of Matter, Transport and Energy, Arizona State University, Tempe Arizona 85287, United States, and [‡]School of Electrical, Computer and Energy Engineering, Arizona State University, Tempe Arizona 85287, United States

ABSTRACT High quality stoichiometric lead sulfide (PbS) wires were synthesized by a simple chemical vapor deposition (CVD) process using pure PbS powder as the material source. Growth mechanisms were systematically investigated under various growth conditions, with three modes of growth identified: direct vapor–liquid–solid (VLS) wire growth nucleating from the substrate surface, bulk PbS crystallites by vapor–solid (VS) deposition, and subsequent VLS growth nucleating on top of the bulk deposition through spontaneously formed catalyst particles. Furthermore, we found that these growth modes can be organized in terms of different levels of supersaturation, with VS bulk deposition dominating at high supersaturation and VLS wire growth on the substrate dominating at low supersaturation. At intermediate supersaturation, the bulk VS deposition can form larger crystallites with domains of similarly oriented wires extending from the flat facets. Both predeposited catalysts and spontaneously formed Pb particles were observed as nucleation catalysts, and their interplay leads to various interesting growth scenarios such as reversely tapered growth with increasing diameter. The VLS growth mechanism was confirmed by the presence of Pb-rich caps revealed in an elaborate cross-sectional transmission electron microscopy (TEM) experiment after focused ion beam milling in a modified lift-out procedure. Temperature-dependent photoluminescence (PL) of PbS wires was performed in the mid-infrared wavelength range for the first time, demonstrating strong light emission from band edge, blue-shifted with increasing temperature. The high optical quality of PbS wires may lead to important applications in mid-infrared photonics. The substrate growth temperature as low as 400 °C allows for silicon-compatible processing for integrated optoelectronics applications.

KEYWORDS: lead sulfide · vapor–liquid–solid growth · chemical vapor deposition · infrared photonics · photoluminescence · supersaturation

PbS is important for a wide range of applications including mid- and near-infrared emission and detection,[1,2] electroluminescence,[3] lasers,[4–7] solar cells,[8] and thermophotovoltaics.[9] As a light emission material with a small band gap of 0.41 eV, PbS has potential for very efficient IR emission due to its nearly symmetric conduction and valence bands. The similar effective masses of electrons and holes near the band edge increases efficiency of electron–hole recombination and reduces the probability of Auger recombination, an important nonradiative process in competition with radiative recombination in narrow gap semiconductors. Recently, PbS nanocrystals also attracted a great deal of attention due to the observation of multiexciton generation, significant to solar cell applications.[10,11] In addition, when alloyed with CdS, the CdPbS ternary alloy is an interesting solar cell material with band gaps spanning from 0.41 to 2.4 eV, the entire spectrum important for solar cells.[12] Specifically for PbS nanowires, several different methods for growth have been demonstrated, including CVD,[13–19] hydrothermal,[20–23] solvothermal,[19,24–27] template-assisted solvothermal,[28,29] and template-assisted electrochemical deposition.[30] The growth of large PbS whiskers with 140 μm width and 400 μm length was reported in 1971 by heating solid bulk PbS in a vacuum chamber.[31] Of the more recent CVD methods, some report growth without intentionally introducing any metal catalyst material,[13–18] while another demonstrates Au as catalyst.[19] Despite great progress made over the past few years, several issues remain before this interesting infrared material can be fully explored for various applications in quasi-one-dimensional form. First, all of these CVD methods use $PbCl_2$ and S powder precursors. The use of $PbCl_2$ in the presence of H_2 gas leads to the formation of HCl which can result in surface roughening by etching.[15] In addition, separate sources of Pb and S require careful balance to produce stoichiometric materials. To emphasize, various morphologies of PbS structures have been observed and are evaluated here in terms of supersaturation. A systematical and unified understanding of various growth modes is essential for controlled synthesis with desired morphologies.

* Address correspondence to cning@asu.edu.

Received for review July 18, 2011 and accepted September 29, 2011.

Published online October 07, 2011
10.1021/nn202704u

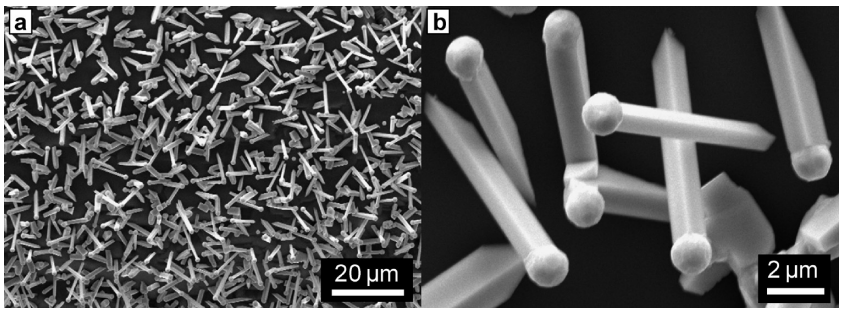

Figure 1. SEM images of as-grown PbS wires with (a) wide area of coverage and (b) direct nucleation from the substrate surface.

TABLE 1. Summary of Growth Conditions and Results (S: Supersaturation)

						observed growth modes			
Figure no.	catalyst	gas	source temp (°C)	substrate temp (°C)	growth time (min)	VLS wires on substrate	VS bulk crystallites	VLS wires on bulk	S
1	none	Ar + 5% H_2	600	400	10	√			low
2	Pb	N_2	730	450	7	√	√		high
3	Au	N_2	800	550	15	√	√		high
4	Pb	N_2	700	500	7	√	√	√	intermediate
5	Pb	N_2	670	500	7		√	√	intermediate

Another important motivation of the present work is extending the optical study of one-dimensional materials to longer wavelengths. Previously we have grown Sb-based narrow gap nanowires and demonstrated lasing at a wavelength of ~1.6 μm using GaSb nanowires.[32] Recently this study was extended to wavelengths below 3 μm using InAs nanowires, which represents the longest wavelength of any nanowires studied so far.[33] So far, there are no reports of the optical study of wire materials with wavelengths longer than 3 μm.

In this paper, we report a simple CVD method for the growth of PbS wires, uniquely utilizing pure PbS powder as the source material to create stoichiometrically matched end-product, eliminating the necessity for separate control of two sources. By systematically studying different growth conditions to achieve various wire and bulk morphologies, we can relate the growth modes to different levels of gas phase supersaturation. Three growth modes were systematically realized, including quasi-one-dimensional VLS growth on the substrate, VS growth of bulk crystallites, and VLS wire growth on top of bulk crystallites through spontaneously formed Pb-catalyst particles. The role of catalyst was studied with and without intentional predeposition of metal. We found that the spontaneous formation of catalyst can lead to dynamic increase of catalyst size during the wire growth process, resulting in reversed tapering of wires with increasing diameter. Although the diameters of these specific wires are larger (from 1 to several micrometers), the growth methods and mechanisms apply to the more general growth of other nanowires with smaller size, since these three growth modes are often seen individually or in various combinations in other growths. To confirm the existence of catalyst caps of a typical VLS growth mode, we performed transmission electron microscopy (TEM)—energy dispersive X-ray spectroscopy (EDS) analysis after a modified focused ion beam (FIB) lift-out procedure. PL results indicate strong mid-IR band-edge emission in a wide temperature range from cryogenic to room temperature with no significant defect emission, indicating high material quality. The temperature-dependent PL shows a blue-shift of spectral peak with increasing temperature, consistent with the known band gap increase with temperature for PbS. Overall, the growth conditions for PbS wires are promising for integration with silicon-based electronics because the relatively low substrate temperature is compatible with CMOS processing (<400 °C).

RESULTS AND DISCUSSION

Growth details are summarized in the Experimental Section. Figures 1 through 5 show many diverse PbS morphologies with the growth conditions summarized in Table 1. The scanning electron microscopy (SEM) images in Figure 1 are typical as-grown PbS wires on Si(100) with no intentionally added catalyst. There are many distinct, individual wires with minimal deposition of other morphologies. The wires have a square cross section with approximately 1 μm diameter and 10 μm length. The number density of wires decreases further downstream along the sample. The wires show no orientation relationship with each other or

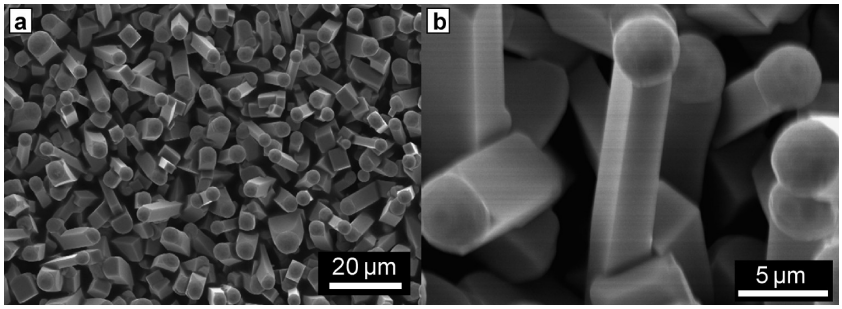

Figure 2. SEM images of as-grown PbS wires with Pb catalyst with (a) dense coverage across the substrate surface and (b) bulk crystallites between the wires.

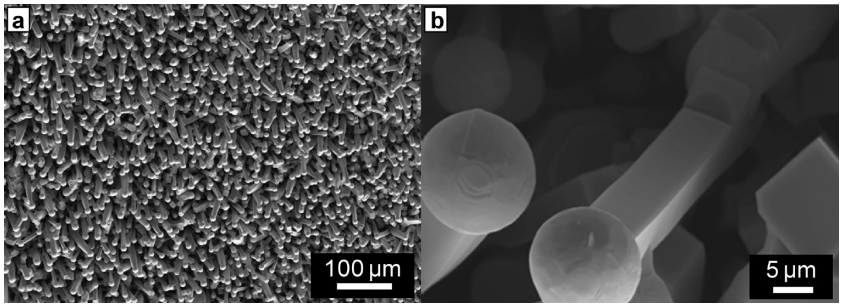

Figure 3. SEM image of as-grown Au-catalyzed PbS wires, (a) tilted 20° from normal and with (b) bulk deposition surrounding wires.

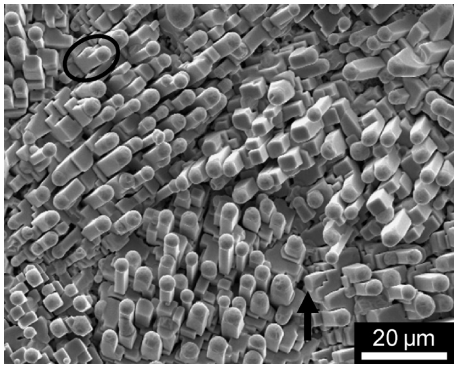

Figure 4. Pb-catalyzed PbS wires with local orientation domains. Arrow (lower right) indicates an area of bulk crystallite deposition. Circle (top left) indicates example of VLS wire growth nucleating on top of bulk.

the substrate, indicating wire nucleation directly from the substrate in random directions. These wires show a larger diameter compared to the values ranging from 30 to 350 nm reported in literature for PbS CVD growth.[13−19] The larger diameters can be especially beneficial for many infrared optical applications since they provide more optically active material or serve as better waveguides for such long wavelengths in the mid-infrared regime.

Growth experiments were also completed with thin Pb or Au catalyst layers deposited prior to the growth process. An approximately 6 nm thick Pb film was evaporated, or about 2 nm of Au was sputtered, onto Si(100) substrates. The Pb-catalyst sample in Figure 2 shows wires with square cross sections, diameters from 3−5 μm, and lengths around 20 μm. The wires are surrounded by bulk crystallite deposition. Figure 3 is a sample with Au catalyst which shows similar wire and bulk morphology as the Pb-catalyst sample in Figure 2. The sample in Figure 4 was grown with Pb catalyst film but at different source and substrate temperatures than Figure 2. It shows domains of similarly oriented wires. Figure 5 represents another set of temperature conditions with Pb catalyst, revealing tapered wires extending from bulk crystallites.

From our growth experiments and characterization, we can conclude several growth modes and associated mechanisms. Their relations in determining the final diverse morphologies can be systematically understood. The VLS wire growth mechanism is a common and well established growth mechanism for wires. A characteristic feature of VLS is a metal-rich round cap at the tip of the wire. As the wire grows, this liquid droplet remains on the top of the wire as solid material crystallizes out of the bottom of the liquid droplet. The liquid droplet serves as the catalyst because it lowers the activation energy of nucleation, and promotes subsequent one-dimensional growth.[34] All of the SEM images show some PbS wires with round caps.

First, it is interesting to understand several possible origins of catalysts and their roles in formation of various morphologies. For the samples without an intentionally added metal catalyst layer, we observe that some Pb is spontaneously formed to supply the required metal catalyst for VLS wire growth. There are two ways that Pb catalyst particles could form depending

on the presence or absence of H_2. In the first case, the H_2 present within the carrier gas could reduce PbS vapor to form volatile sulfur compounds, isolating elemental Pb atoms to be carried downstream, as similar behavior has been observed for the reduction of $PbCl_2$ in PbS CVD growth.[15−18] The Pb vapor then condenses on the substrate, becoming the liquid catalyst for subsequent VLS growth of PbS wires. The importance of H_2 gas for consistent growth of PbS wires catalyzed by spontaneously generated Pb was identified by Bierman *et al.*, and they used SEM EDS to verify the presence of a Pb-rich cap of a PbSe wire with similar size and morphology to our wires.[15] This mechanism is further verified by the TEM EDS analysis of our PbS wires as will be shown later. In the second case without H_2 gas such as in some of our experiments, PbS could incongruently sublimate to continually provide catalyst in the form of elemental Pb vapor.

For samples grown with predeposited catalyst, there are two sources of catalyst metal for the VLS growth: the predeposited layer on the substrate and the spontaneously formed catalyst particles as described above. PbS wires nucleated by Pb, either predeposited or spontaneously generated, are self-catalyzed, meaning that the metal catalyst is an element of the semiconductor compound to be grown as opposed to a foreign metal such as Au.

If the conditions are such that the energy required for vapor incorporation into the VLS liquid droplet is similar to that of the energy required for vapor to form a critical nucleation cluster directly on the substrate surface, then wire growth and bulk growth could occur simultaneously, although possibly at different rates. The Vapor−Solid (VS) process is the proposed mechanism for the growth of bulk crystallites with flat facets without metal caps, see Figure 2b, Figure 3b, Figure 4 (arrow), and Figure 5. In VS process, the source materials condense to the substrate and the molecules are arranged to maintain structural symmetry, creating a nucleation center.[35] Additional vapor molecules incorporate directly into the solid to form the lowest energy surfaces possible, which tend to be flat facets. As in Figure 4, the wires with round caps are taller than the surrounding flat crystallites, indicating that the quasi-one-dimensional VLS growth rate is faster than direct incorporation into the solid by VS.

A third growth mode, VLS wire growth on bulk-like crystallites, is proposed to account for the SEM evidence of wires connected directly to PbS bulk crystallites. In this case, wires are nucleated from the spontaneously formed catalyst particles that developed on top of the already formed bulk crystallites. Since the base of the wire is sometimes surrounded by bulk crystallites as in Figure 2b, Figure 3b and Figure 4, it is not always possible to definitively distinguish which wires are nucleated by the original predeposited metal or by the incoming Pb vapor. Figure 5 shows an

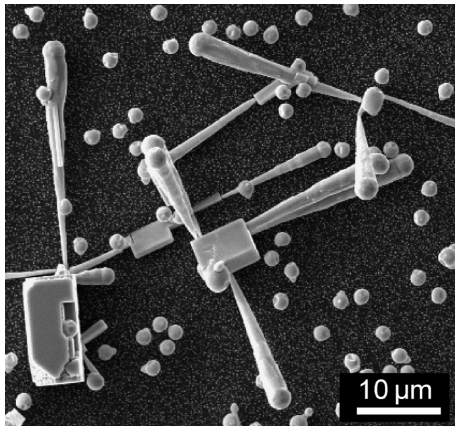

Figure 5. VLS growth of wires on top of PbS bulk. Size of Pb droplet increases with growth, thus increasing wire diameter from 500 nm to 2 μm.

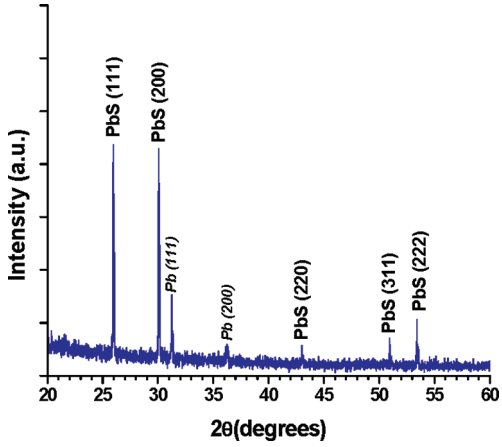

Figure 6. XRD of as-grown PbS wires indexed to corresponding reference peaks.

area with less dense bulk deposition and individual reversely tapered wires clearly nucleated from a central bulk piece of PbS. The diameter of the wire increases with growth, from 500 nm to 2 μm. This is consistent with the proposed mechanism of spontaneous formation of Pb catalyst, whereby continually incoming elemental Pb adds to the existing catalyst cap. The liquid droplet, which defines the diameter of the growing wire, is continuously increasing in volume, thus the diameter of the wire increases.[36−38] In both Figure 4 and Figure 5, an orientation relationship is observed between the bulk and the wires nucleating on top. We believe that the VLS wires on top of bulk crystallize homoepitaxially to the flat PbS surface below as has been verified for other materials systems including GaSb.[39] In summary, we divide observed growth into three categories: VLS wires nucleated directly from the substrate, VS of bulk crystallites, and VLS wire growth nucleated by spontaneously formed Pb on top of the bulk crystallites.

To investigate the favorable growth conditions for each growth mode, the samples were organized by

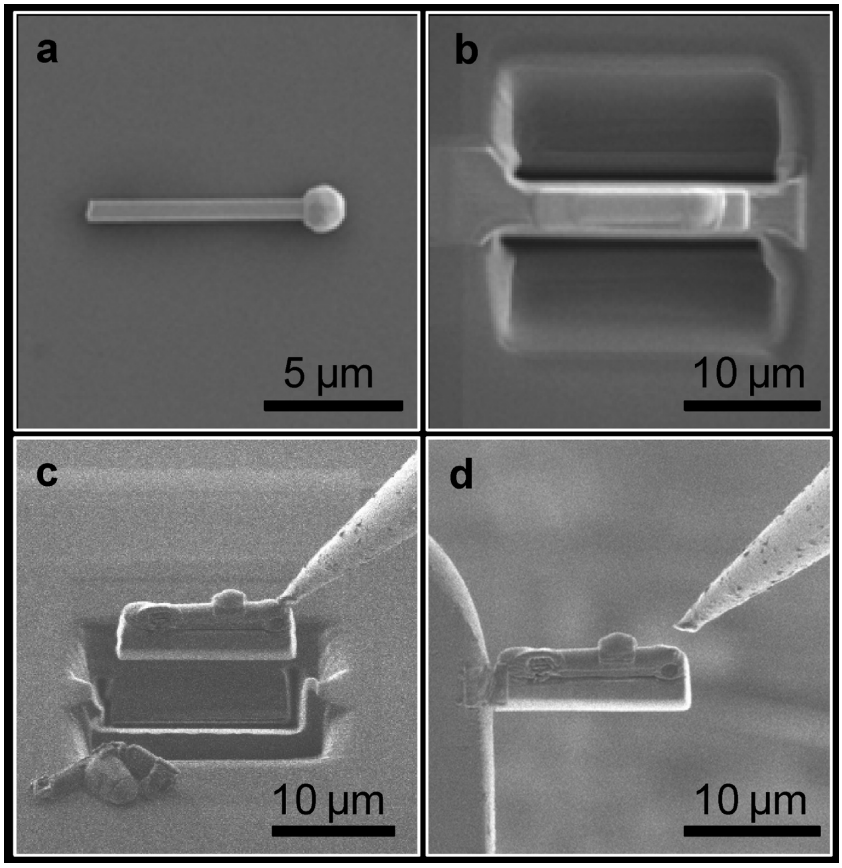

Figure 7. Representative SEM images of FIB processing to create TEM specimen: (a) wire dispersion on a clean Si substrate; (b) encasement of the wire with Pt and milling trenches on either side; (c) lift-out using Pt tip; and (d) attachment to TEM grid.

their distinct PbS gas phase supersaturations. Gas phase supersaturation, S, is formally defined as[40]

$$S = \frac{p - p_0}{p_0}$$

where p is the actual gas phase pressure and p_0 is the equilibrium vapor pressure. Supersaturation at the substrate can be estimated by considering the magnitude of the source temperature and the difference between the source and substrate temperatures. The magnitude of the source temperature controls the rate of sublimation from the source powder, as the vapor pressure of PbS increases with temperature.[41] When the source temperature is low (~600 °C), there is very little vapor available to move downstream to the lower temperature substrate zone. This results in low supersaturation over the substrate. Nearly all of the precipitation from vapor phase can be accommodated by the VLS liquid droplets. The rate of incorporation of new material into the liquid particle is much larger than incorporation onto the substrate surface. When the source temperature is high (>650 °C), large amounts of vapor are available to move downstream. If this vapor transitions to a moderately high substrate temperature zone, the supersaturation is intermediate. The precipitating vapor can crystallize into both VS bulk crystallites and VLS wires. There is substantial thermal energy at the substrate that provides high mobility to the atoms on the substrate so they can arrange into large grains or domains of similar orientation as in Figure 4. Subsequently, VLS growth can occur on top of these ordered bulk crystallites as previously described. If large amounts of vapor immediately encounter a much lower temperature zone, there will be high supersaturation at the substrate. The vapor crystallizes rapidly, favoring VS growth of bulk crystallites. Transition of the PbS vapor to solid occurs too rapidly to be completely accommodated by VLS liquid particles. Samples grown at even higher supersaturations than listed here generally showed only bulk crystallite morphology. In general, these samples grown at different supersaturation conditions reveal a complex growth process with the possibility for three simultaneous growth modes.

X-ray diffraction (XRD) was performed on PbS wire samples with a representative scan shown in Figure 6. The peaks can be indexed to PbS and Pb as labeled. There are no undesirable oxide phases detected. The PbS phase has cubic rocksalt structure with calculated lattice parameter of 0.59 nm which matches well with the known PbS lattice parameter of 0.5934 nm (JCPDS card no. 01-077-0244). The remaining peaks index to Pb with lattice parameter of 0.49 nm which is in good agreement with the known lattice parameter of

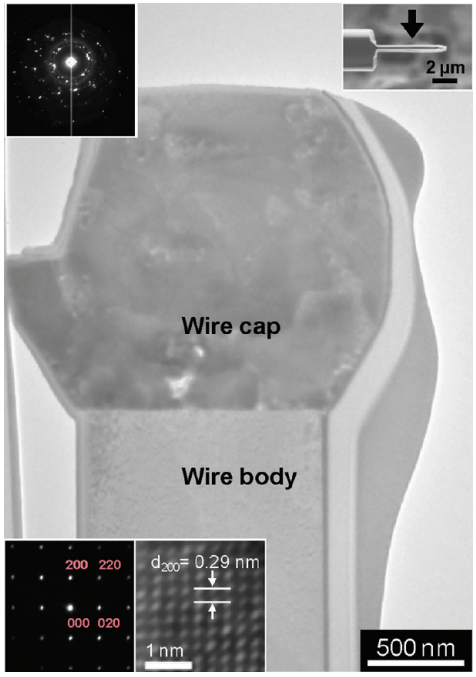

Figure 8. TEM image of thinned PbS. Inset top right: side-view SEM image of thinned wire with arrow indicating TEM beam direction. Inset top left: diffraction pattern from wire cap. Inset bottom left: diffraction pattern and high resolution TEM of wire body, both confirming ⟨100⟩ growth direction.

0.49493 nm (JCPDS card no. 03-065-2873). The sharp peaks indicate high quality crystal.

To confirm the location of elemental Pb detected by XRD, TEM was necessary to individually probe wires grown without intentionally added catalyst and their round caps. Typical nanowires can be directly dispersed onto a holey carbon grid for TEM analysis, but due to the large diameter of these PbS wires, auxiliary processing was necessary to create a TEM specimen with electron transparency. The FIB thinning process is based on a common lift-out procedure, but modified for wires. First PbS wires (grown by conditions of Figure 1) were dispersed onto a clean Si substrate (Figure 7a). The wires were encased in layers of platinum to protect the wire during lift-out. Electron beam induced deposition was used for the first layer of Pt to protect the PbS wire because the electron beam generally does not ablate material; ion beam induced deposition of Pt with a much faster deposition rate then completed the encasement. Trenches were milled on either side of the wire using the Gallium ion beam milling (Figure 7b). The Pt tip was welded to the Pt encasing the wire and the whole wire and Pt structure was lifted out of the Si wafer (Figure 7c). The wire structure was attached to a TEM grid using more Pt, and the Pt tip was disconnected from the structure using Ga ion beam milling (Figure 7d). Stage tilt and rotation positioned the structure for perpendicular thinning on either side. The Ga ion beam current and energy

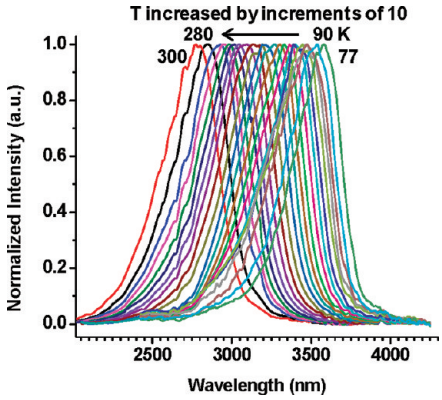

Figure 9. PL spectra measured at various temperatures showing band edge emission with blue-shift with increasing temperature. Dips are due to atmospheric absorption.

were decreased as milling continued to minimize damage to the PbS structure. The final PbS structure is approximately 50 nm thick with original wire material in the TEM beam direction and residual Pt on the wire sidewalls (inset, Figure 8). The FIB process for TEM sample preparation exposes the wire cap and body for separate elemental and crystallographic analysis.

Figure 8 contains a TEM image of the PbS wire and cap. The diffraction pattern of the round cap shows rings of spots due to the polycrystalline grain structure. The diffraction pattern from the PbS wire shows the ⟨100⟩ zone axis, with the (200) diffraction spots parallel to the wire sidewall, indicating that the wire growth direction is ⟨100⟩. This is consistent with the square cross section of the wires, which is the equilibrium shape for a wire with (200) planes constructing the sidewalls of the structure. The high resolution TEM image shows lattice fringe spots with an average spacing of 0.29 nm which corresponds well to the actual 0.2967 nm (200) spacing of bulk PbS, also confirming ⟨100⟩ growth direction.

EDS measurements were taken at the cap and body regions of the wire. There are some challenges involved in the EDS analysis of PbS due to overlap between the Pb Mα absorption edge and S Kα line. For this analysis, it was assumed that the peak around those energies is attributed to S K, and the Pb L line was taken as the Pb signal strength for quantitative calculation. Strong peaks from Pb and S are apparent in the EDS spectrum with no unexpected impurity elements (Cu signal is from the TEM grid and Ga is due to residual Ga implantation from FIB processing, see Supporting Information). According to quantitative analysis, the molar ratio of S to Pb in the wire body is 1:1.1, which is consistent with the expected stoichiometric PbS, and is within experimental error due to X-ray peak overlap and FIB processing damage. This amount of deviation from stoichiometry is similar to other reported quantitative EDS analysis of PbS nanostructures.[19,42] The molar ratio of S to Pb in the round wire cap is 1:8.4. This

indicates that the cap contains some PbS in addition to significant amounts of metallic Pb. The measurement of the isolated Pb-rich cap is consistent with the proposed wire growth mechanism of nucleation by spontaneously formed Pb and subsequent VLS growth.

PL is one of the most important methods of characterization for materials with optoelectronic applications. Unfortunately PL measurement in the mid-infrared range is more challenging due to typically weak emission and equipment availability. Previous literature reports of PL measurements on PbS wires are limited to quantized structures with PL emission extremely blue-shifted away from the bulk IR value. The wires studied by Paleta *et al*. have diameters of 1.8 nm with band-edge emission at 480 nm.[27] Wu *et al*. reported PbS nanowires with 30 nm diameter with PL emission peaks at 365 and 678 nm.[30] The optical properties of these PbS structures are completely different than the mid-infrared optical properties of the PbS wires in this work. Due to the importance of PbS as a material for mid-infrared light sources and detectors for many applications, it is very interesting to study the optical properties of PbS. The large wires obtained in our growth do not show any quantization and allow the original bulk band gap emission in the mid-infrared wavelength range to be studied. As seen in Figure 9, very strong band-edge emission was observed with no defect emission, indicating high quality wires. The PL peak shows an obvious blue shift with increasing temperature, which is consistent with the known behavior of bulk PbS.[43] Contrasting to that of typical semiconductors, the band gap of PbS increases with increasing temperature. As previously mentioned, the strong light emission of PbS is a result of symmetric band structure which enhances the radiative process and inhibits the nonradiative processes such as Auger recombination. The high crystal quality and strong light emission make PbS an appealing material for photonic applications in the mid-infrared wavelength range. This is especially important since emission sources in the wavelength range around 3 μm are rare and typically very weak due to various competing nonradiative processes.

CONCLUSIONS

We have demonstrated a simple CVD synthesis method of producing large, high quality PbS wires utilizing pure PbS powder as the source material. The wires were systematically characterized by various analysis tools, including TEM, EDS, XRD, and temperature-dependent PL to confirm the chemical composition and crystal structure. The ⟨100⟩ growth direction and the VLS growth mechanism were confirmed by FIB thinning, subsequent TEM imaging, and TEM EDS, showing the Pb-rich cap. Multiple catalyst sources, both predeposited or spontaneously formed, contribute to the growth of PbS wires.

Growth modes were systematically investigated under different growth conditions, including VLS growth of wires directly from the substrate, VS deposition of bulk crystallites, and subsequent VLS wire growth on top of the bulk crystallites. We were able to relate different levels of supersaturation to these growth modes, with VLS on the substrate dominating at low supersaturation and VS growth of bulk crystallites dominating at high supersaturation. The effect of supersaturation on the appearance of wires and bulk crystallites is important to CVD growth of various morphologies and compositions of nanostructures. We believe that such systematic understanding of various growth modes will help our efforts in eventually achieving synthesis by design, or achieving nanowires of a given morphology by controlled experimental conditions. Temperature-dependent PL showed strong band-edge emission, even up to room temperature, which is essential for applications requiring strong mid-infrared light emission such as lasers.

We note that even though most of the wires shown in this paper are relatively large with diameters from 1 to several micrometers, smaller wires with diameters of several hundreds of nanometers have also been observed, especially at the early stage of tapered growth. More importantly, since the various morphologies discussed here have been observed in the growth of other materials and with much smaller sizes, we believe that the overall understanding of the growth mechanisms are applicable more generally to other materials of nanometer size. Our focus on somewhat larger nanowires was also motivated by our intended applications in optoelectronics, in which large wires in this long wavelength range are required to provide sufficient active materials and to act as better waveguides. Finally the CVD growth reported here can occur at a relatively low substrate temperature of no higher than 400 °C, compatible with CMOS processing temperatures. Such conditions can potentially allow for the growth of mid-infrared photonic devices directly on the backside of CMOS chips for detectors and laser applications.

EXPERIMENTAL SECTION

Sample Synthesis. PbS wires were grown in a horizontal quartz tube furnace (Lindberg/Blue M Three-Zone Tube Furnace) with stoichiometric PbS powder (Strem Chemicals, Lead(II) sulfide (99.999%)) as the source material in the high temperature zone (from 600 to 800 °C). The substrate, Si (100) with or without

intentionally added catalysts (Au or Pb), was placed on a quartz plate in the low temperature zone (from 400 to 550 °C). The system was evacuated to a pressure of less than 100 mTorr. Under flowing N_2 or Ar + 5% H_2 at 50 sccm, the pressure was maintained around 15 Torr. After the furnace reached the set temperatures in the high and low temperature zones, the PbS source boat was inserted into the center of the furnace *via* a magnetic loading rod. The PbS source powder was sublimated in the high temperature zone, and deposited onto the substrates in the low temperature zone about 10 cm downstream.

Characterization. SEM imaging was performed using a Philips XL-30 field-emission SEM. XRD data was collected on a PANalytical X'Pert Pro Materials Research X-ray diffractometer equipped with CuKa radiation (λ = 0.154178 nm). The FIB sample preparation was performed on a FEI FIB/SEM Nova 200 NanoLab UHR FEG. TEM was performed on a JEOL JEM-2010 high-resolution transmission electron microscopy at 200 kV, equipped with a Link EDS detector. The PL data was collected with a mid-IR micro-PL setup with a passively mode-locked Ti:sapphire laser (SpectraPhysics Tsunami, 790 nm, 150 fs pulse duration, 80 MHz repetition rate). Samples were placed in a microscope cryostat under vacuum with liquid nitrogen cooling for low temperature PL measurements. The excitation laser was directed to the samples at 45° from the substrate surface normal. The emission was detected by a liquid nitrogen cooled InSb photodiode detector. An optical chopper in the excitation laser beam and a lock-in amplifier connected to the InSb photodiode suppressed detector noise. Compressed nitrogen gas was used to purge the PL light path to reduce water and air absorption.

Acknowledgment. We gratefully acknowledge the use of facilities within the LeRoy Eyring Center for Solid State Science at Arizona State University, and specifically thank G. Tam (FIB processing), D. Wright, T. Karcher, and Z. Liu. We also acknowledge S. Aithal for assistance in initial furnace setup. This work is supported by an ARO grant (W911NF-08-1-0471) under M. Gerhold. P.L.N. was initially supported by the Ira A. Fulton Schools of Engineering Dean's Fellowship.

Supporting Information Available: Schematic furnace diagram; EDS data. This material is available free of charge *via* the Internet at http://pubs.acs.org.

REFERENCES AND NOTES

1. Bakueva, L.; Gorelikov, I.; Musikhin, S.; Zhao, X. S.; Sargent, E. H.; Kumacheva, E. PbS Quantum Dots with Stable Efficient Luminescence in the Near-IR Spectral Range. *Adv. Mater.* **2004**, *16*, 926–929.
2. Pentia, E.; Pintilie, L.; Matei, I.; Botila, T.; Pintilie, I. Combined Chemical-Physical Methods for Enhancing IR Photoconductive Properties of PbS Thin Films. *Infrared Phys.Technol.* **2003**, *44*, 207–211.
3. Bakueva, L.; Musikhin, S.; Hines, M. A.; Chang, T. W. F.; Tzolov, M.; Scholes, G. D.; Sargent, E. H. Size-Tunable Infrared (1000−1600 nm) Electroluminescence from PbS Quantum-Dot Nanocrystals in a Semiconducting Polymer. *Appl. Phys. Lett.* **2003**, *82*, 2895–2897.
4. Sukhovatkin, V.; Musikhin, S.; Gorelikov, I.; Cauchi, S.; Bakueva, L.; Kumacheva, E.; Sargent, E. H. Room-Temperature Amplified Spontaneous Emission at 1300 nm in Solution-Processed PbS Quantum-Dot Films. *Opt. Lett.* **2005**, *30*, 171–173.
5. Tamulaitis, G.; Gulbinas, V.; Kodis, G.; Dementjev, A.; Valkunas, L.; Motchalov, I.; Raaben, H. Optical Nonlinearities of Glass Doped with PbS Nanocrystals. *J. Appl. Phys.* **2000**, *88*, 178–182.
6. Dantas, N. O.; Qu, F.; Silva, R. S.; Morais, P. C. Anti-Stokes Photoluminescence in Nanocrystal Quantum Dots. *J. Phys. Chem. B* **2002**, *106*, 7453–7457.
7. Koguchi, N; Takahashi, S. Double-Heterostructure $Pb_{1-x-y}Cd_xSr_yS$/PbS/$Pb_{1-x-y}Cd_xSr_yS$ Lasers Grown by Molecular Beam Epitaxy. *Appl. Phys. Lett.* **1991**, *58*, 799–800.
8. Plass, R.; Pelet, S.; Krueger, J.; Gratzel, M.; Bach, U. Quantum Dot Sensitization of Organic−Inorganic Hybrid Solar Cells. *J. Phys. Chem. B* **2002**, *106*, 7578–7580.
9. Dhere, N. G. Appropriate Materials and Preparation Techniques for Polycrystalline-Thin-Film Thermophotovoltaic Cells. *AIP Conf. Proc.* **1997**, *401*, 423–442.
10. Ellingson, R. J.; Beard, M. C.; Johnson, J. C.; Yu, P.; Micic, O. I.; Nozik, A. J.; Shabaev, A.; Efros, A. L. Highly Efficient Multiple Exciton Generation in Colloidal PbSe and PbS Quantum Dots. *Nano Lett.* **2005**, *5*, 865–871.
11. Klimov, V. I. Mechanisms for Photogeneration and Recombination of Multiexcitons in Semiconductor Nanocrystals: Implications for Lasing and Solar Energy Conversion. *J. Phys. Chem. B* **2006**, *110*, 16827–16845.
12. Caselli, D. A.; Ning, C. Z. High-Performance Laterally-Arranged Multiple-Bandgap Solar Cells Using Spatially Composition-Graded $Cd_xPb_{1-x}S$ Nanowires on a Single Substrate: A Design Study. *Opt. Express* **2011**, *19*, A686–A694.
13. Ge, J. P.; Wang, J.; Zhang, H. X.; Wang, X.; Peng, Q.; Li, Y. D. Orthogonal PbS Nanowire Arrays and Networks and Their Raman Scattering Behavior. *Chem.—Eur. J.* **2005**, *11*, 1889–1894.
14. Afzaal, M.; O'Brien, P. Silica Coated PbS Nanowires. *J. Mater. Chem.* **2006**, *16*, 1113–1115.
15. Bierman, M. J.; Lau, Y. K. A.; Jin, S. Hyperbranched PbS and PbSe Nanowires and the Effect of Hydrogen Gas on Their Synthesis. *Nano Lett.* **2007**, *7*, 2907–2912.
16. Bierman, M. J.; Lau, Y. K. A.; Kvit, A. V.; Schmitt, A. L.; Jin, S. Dislocation-Driven Nanowire Growth and Eshelby Twist. *Science* **2008**, *230*, 1060–1063.
17. Lau, Y. K. A.; Chernak, D. J.; Bierman, M. J.; Jin, S. Formation of PbS Nanowire Pine Trees Driven by Screw Dislocations. *J. Am. Chem. Soc.* **2009**, *131*, 16461–16471.
18. Lau, Y. K. A.; Chernak, D. J.; Bierman, M. J.; Jin, S. Epitaxial Growth of Hierarchical PbS Nanowires. *J. Mater. Chem.* **2009**, *19*, 934–940.
19. Jang, S. Y.; Song, Y. M.; Kim, H. S.; Cho, Y. J.; Seo, Y. S.; Jung, G. B.; Lee, C. W.; Park, J.; Jung, M.; Kim, J.; *et al.* Three Synthetic Routes to Single-Crystalline PbS Nanowires with Controlled Growth Directions and Their Electrical Transport Properties. *ACS Nano* **2010**, *4*, 2391–2401.
20. Wang, S.; Pan, A.; Yin, H.; He, Y.; Lei, Y.; Xu, Z.; Zou, B. Synthesis of PbS Microcrystals *via* a Hydrothermal Process. *Mater. Lett.* **2006**, *60*, 1242–1246.
21. Kuang, D.; Xu, A.; Fang, Y.; Liu, H.; Frommen, C.; Fenske, D. Surfactant-Assisted Growth of Novel PbS Dendritic Nanostructures *via* Facile Hydrothermal Process. *Adv. Mater.* **2003**, *15*, 1747–1750.
22. Chen, J.; Chen, L.; Wu, L. M. The Solventless Syntheses of Unique PbS Nanowires of X-Shaped Cross Sections and the Cooperative Effects of Ethylenediamine and a Second Salt. *Inorg. Chem.* **2007**, *46*, 8038–8043.
23. Ding, B.; Shi, M.; Chen, F.; Zhou, R.; Deng, M.; Wang, M.; Chen, H. Shape-Controlled Syntheses of PbS Submicro-/Nano-Crystals *via* Hydrothermal Method. *J. Cryst. Growth* **2009**, *311*, 1533–1538.
24. Saraidarov, T.; Reisfeld, R.; Sashchiuk, A.; Lifshitz, E. Synthesis and Characterization of PbS Nanorods and Nanowires. *Physica E* **2007**, *37*, 173–177.
25. Wang, Z.; Zhao, B.; Zhang, F.; Mao, W.; Qian, G.; Fan, X. Novel Single-Crystal PbS Nanowires Directed by [200]. *Mater. Lett.* **2007**, *61*, 3733–3735.
26. Yong, K. T.; Sahoo, Y.; Choudhury, K. R.; Swihart, M. T.; Minter, J. R.; Prasad, P. N. Control of the Morphology and Size of PbS Nanowires using Gold Nanoparticles. *Chem. Mater.* **2006**, *18*, 5965–5972.
27. Patla, I.; Acharya, S.; Zeiri, L.; Israelachvili, J.; Efrima, S.; Golan, Y. Synthesis, Two-Dimensional Assembly, and Surface Pressure-Induced Coalescence of Ultranarrow PbS Nanowires. *Nano Lett.* **2007**, *7*, 1459–1462.
28. Gao, F.; Lu, Q.; Liu, X.; Yan, Y.; Zhao, D. Controlled Synthesis of Semiconductor PbS Nanocrystals and Nanowires Inside Mesoporous Silica SBA-15 Phase. *Nano Lett.* **2001**, *1*, 743–748.
29. Mukherjee, P. K.; Chatterjee, K.; Chakravorty, D. Semiconductor to Metal Transition in PbS Nanowires Grown in Mica Channels. *Phys. Rev. B* **2006**, *73*, 035414.

30. Wu, C.; Shi, J. B.; Chen, C. J.; Lin, J. Y. Synthesis and Optical Properties of Ordered 30 nm PbS Nanowire Arrays Fabricated into Sulfuric Anodic Alumina Membrane. *Mater. Lett.* **2006**, *60*, 3618–3621.
31. Patel, A. R.; Sangwal, K. Growth and Etching of PbS Whiskers from the Vapour Phase. *J. Cryst. Growth* **1971**, *8*, 282–284.
32. Chin, A. H.; Vaddiraju, S.; Maslov, A. V.; Ning, C. Z.; Sunkara, M. K.; Meyyappan, M. Near-Infrared Semiconductor Subwavelength-Wire Lasers. *Appl. Phys. Lett.* **2006**, *88*, 163115.
33. Sun, M. H.; Leong, E. S. P.; Chin, A. H.; Ning, C. Z.; Cirlin, G. E.; Samsonenko, Y. B.; Dubrovskii, V. G.; Chuang, L.; Chang-Hasnain, C. Photoluminescence Properties of InAs Nanowires Grown on GaAs and Si Substrates. *Nanotechnology* **2010**, *21*, 335705.
34. Kolasinski, K. W. Catalytic Growth of Nanowires: Vapor–Liquid–Solid, Vapor–Solid–Solid, Solution–Liquid–Solid and Solid–Liquid–Solid Growth. *Curr. Opin. Solid State Mater Sci.* **2006**, *10*, 182–191.
35. Kar, S.; Chaudhuri, S. Shape Selective Growth of CdS One-Dimensional Nanostructures by a Thermal Evaporation Process. *J. Phys. Chem. B* **2006**, *110*, 4542–4547.
36. Mattila, M.; Hakkarainen, T.; Lipsanen, H.; Jiang, H.; Kauppinen, E. I. Catalyst-Free Growth of In(As)P Nanowires on Silicon. *Appl. Phys. Lett.* **2006**, *89*, 063119.
37. Colombo, C.; Spirkoska, D.; Frimmer, M.; Abstreiter, G.; Fontcuberta i Morral, A. Ga-Assisted Catalyst-Free Growth Mechanism of GaAs Nanowires by Molecular Beam Epitaxy. *Phys. Rev. B* **2008**, *77*, 155326.
38. Plissard, S.; Dick, K. A.; Larrieu, G.; Godey, S.; Addad, A.; Wallart, X.; Caroff, P. Gold-Free Growth of GaAs Nanowires on Silicon: Arrays and Polytypism. *Nanotechnology* **2010**, *21*, 385602.
39. Vaddiraju, S.; Sunkara, M. K.; Chin, A. H.; Ning, C. Z.; Dholakia, G. R.; Meyyappan, M. Synthesis of Group III Antimonide Nanowires. *J. Phys. Chem. C* **2007**, *111*, 7339–7347.
40. Ye, C.; Fang, X.; Hao, Y.; Teng, X.; Zhang, L. Zinc Oxide Nanostructures: Morphology Derivation and Evolution. *J. Phys. Chem. B* **2005**, *109*, 19758–19765.
41. Botor, J.; Milkowska, G.; Konieczny, J. Vapour Pressure and Thermodynamics of PbS. *Thermochim. Acta* **1989**, *137*, 269–279.
42. Jana, S.; Goswami, S.; Nandy, S.; Chattopadhyay, K. K. Synthesis of Tetrapod like PbS Microcrystals by Hydrothermal Route and its Optical Characterization. *J. Alloys Compd.* **2009**, *481*, 806–810.
43. Preier, H. Recent Advances in Lead-Chalcogenide Diode Lasers. *Appl. Phys.* **1979**, *20*, 189–206.